

---

# A Multichannel, High-Resolution, UV Spectrometer for Laser-Fusion Applications

## Introduction

The 60-beam OMEGA laser system is used for inertial confinement fusion (ICF) studies.<sup>1</sup> The configuration of each of the 60 beams should be exactly the same to produce the most-uniform ICF implosions.<sup>2</sup> A shaped infrared (IR) ( $\lambda = 1053$  nm) pulse is generated from a single master oscillator and fed into 60 beamlines with large Nd:glass amplifiers.<sup>3</sup> Each beamline produces approximately 800 J of IR light in a 1-ns pulse. The frequency of the IR light is tripled in a series of KDP crystals to produce UV light at 351 nm, which is used to illuminate the ICF target. An important feature of this laser system is that spectral broadening can be deliberately imposed on the emitted radiation using a technique called smoothing by spectral dispersion (SSD).<sup>4</sup> This is done to produce a more-uniform, time-integrated illumination profile at the target. The imposed bandwidth has a width of 1.2 nm in the IR, which exceeds the acceptance bandwidth of the potassium dihydride phosphite (KDP) crystals used for frequency tripling.<sup>5</sup> To overcome this problem, each beam has two tripling crystals that are angularly detuned with respect to the direction of propagation.<sup>6</sup> The acceptance bandwidth of the combined crystals is large enough to efficiently convert the SSD pulses. To maintain the highest conversion efficiency, the angular detuning of the KDP crystals must be controlled to approximately  $100 \mu\text{rad}$ . Mistuned crystals decrease the UV conversion efficiency and change the spectra of the converted light. A procedure has been developed to tune the crystals by looking at the conversion efficiency on nine laser shots; however, the tuning can drift with time, and checks of individual beamlines have revealed that the spectra were different. Figure 101.48 illustrates the differences in spectra between two beamlines. To facilitate a more-accurate tuning procedure, a spectrometer was built to measure the UV spectra of all 60 beams on all OMEGA shots. This article describes that spectrometer.

In addition to the bandwidth imposed by the SSD system, there is an intrinsic source of bandwidth on the OMEGA system. If the intensity of a laser pulse varies rapidly in time, the nonlinear index of refraction produces a time-varying phase.<sup>7</sup> The time-varying phase produces a wavelength shift.

The spectral structures associated with these intrinsic wavelength shifts have typical widths of 3 picometers (pm). The ability to understand and control this intrinsic bandwidth was a secondary motivation for building this spectrometer.

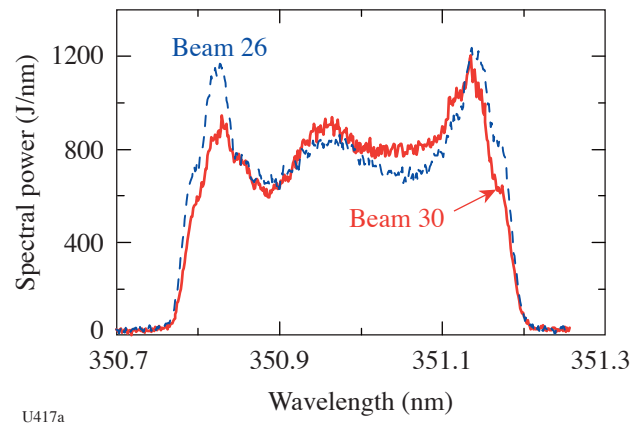


Figure 101.48

The spectra, with SSD on, vary from beam to beam on the same shot. The dashed curve is for beam 26 on shot 35711, and the solid curve is for beam 30 on the same shot.

The dual missions mentioned above determined the specifications of the spectrometer that was constructed. The spectrometer had to be able to acquire at least 60 complete spectra in a single shot. To allow for the possibility of corrupt channels and to incorporate *in-situ* wavelength calibration, an imaging spectrometer was constructed to accommodate 63 channels. Each channel must span a 0.5-nm bandwidth around  $\lambda = 351.01$  nm to be capable of viewing the entire SSD-broadened spectra. With SSD turned off, the spectrometer must be able to resolve spectral features of the order of 3 pm. The light that feeds the spectrometer will come from a small fraction of the light from each beamline that is split off for diagnostic purposes (about  $1 \mu\text{J}$  on a full-energy shot). The total UV energy per beamline on OMEGA can range from 10 to 500 J. The fraction of light that is split off is linearly dependent on the total beam energy, so the detection system must be able to accommodate signal levels that vary by a factor of 50.

### Spectrometer Layout

The physical layout of the spectrometer is shown in Fig. 101.49. The input to the spectrometer comes from 60 fiber bundles. Each fiber bundle consists of three 300- $\mu\text{m}$ , UV-transmitting, step-index fibers.<sup>8</sup> The fiber bundles are attached to an integrating sphere, which is illuminated with a portion of the light from each beamline. Three fibers are used to increase the light coupled out of the integrating sphere. The fiber bundles attach to an input manifold. Within the manifold, three fibers from each bundle are realigned into a linear array and coupled into a UV-transmitting, fused-silica bar  $10 \times 1.2 \times 0.4 \text{ mm}^3$ , along the 1.2-mm dimension. The bar, which is aluminized on all four sides with a 10-nm edge, acts as an optical homogenizer via multiple reflections off the metallized sides. The light emerging from the fiber should be approximately spatially uniform and have a Gaussian dependence on angle. The homogenizer will cause the high-angle rays that have the lowest uniformity to undergo at least two reflections from the sides, thus increasing the uniformity of the output radiation. This assembly constitutes a single channel, which is the input to the spectrometer. Twenty-one of these channels are arranged in a line. The center channel is fed with a neon pencil lamp, which provides a wavelength fiducial for calibrating the wavelength. The entire manifold consists of three lines of 21 channels separated by 10.4 mm. In between the lines are three uniform bars that can be used to flat-field the instrument.

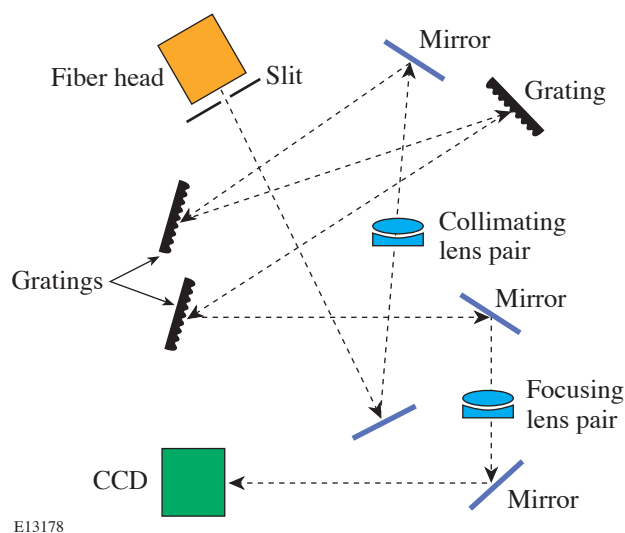


Figure 101.49

The layout of the spectrometer. The light from the fiber bundles passes through a slit array and a pair of collimating lenses before reflecting off of four mirrors and three gratings. A second pair of lenses focuses the light onto a CCD (charge-coupled device).

The resolution of the spectrometer would be limited by the 0.4-mm width of the bar unless the field of view is further limited. Unlike the adjustable slit commonly employed in spectrometers, the resolution of this instrument is selected from a fixed set of slit widths. The manifold sits behind a metallized fused-silica plate. The side of the plate facing the fiber manifold is coated with chromium. The backside is antireflection (AR) coated for UV light. The chromium was photolithographically etched with three sets of slits. Each set contained four slit openings: 10, 20, 40, and 60  $\mu\text{m}$ . The plate sits on a computer-controlled linear stage that allows the selection of a single slit opening for all channels. The diffusing bars provide a uniform light source for illuminating the slit. The bars are at least six times larger than the slit width. By recording the slit opening for each shot, the response of the instrument can be photometrically calibrated.

Table 101.V gives the position and properties of each optical element in the path between the fiber manifold and the CCD (charge-coupled-device) detector. After passing through the slit, the light reflects off of a flat dielectric mirror. Four mirrors are used in the instrument to create a folded optical path. The folded path enables us to compress the instrument, with a total optical path length of greater than 5 m, onto a breadboard 1.2 m on an edge.

The optical system has a total demagnification factor of 0.87; therefore the slits at the input of the system appear smaller at the detector plane. The imaging is done with refractive optics.<sup>9</sup> Four lenses are arranged in two pairs: a collimating pair and a focusing pair. The focus can be adjusted by means of a micrometer that controls the separation of each pair of lenses. Many spectrometers use reflective optics to image the light through the instruments to avoid chromatic aberrations associated with the refractive elements; however, this instrument has a limited spectral range of 0.6 nm centered about 351 nm. Over this spectral range, spectral dispersion in the fused silica can be ignored. The index of refraction changes by less than one part in  $10^5$  over this wavelength range. For the optical system described here, the point-spread function at the CCD detector, due to chromatic aberration, was calculated at three wavelengths (350.7 nm, 351.0 nm, and 351.3 nm) and found to be 11  $\mu\text{m}$ , 6  $\mu\text{m}$ , and 12  $\mu\text{m}$ , respectively, on axis. This means the resolution changes across the spectral range from 1.8 pm to 1.4 pm to 1.9 pm. The advantage of using refractive optics is that the imaging can be done on axis, which allows a wider field of view (FOV) than off-axis imaging. The large FOV is needed because the spatial extent of the fiber manifold is  $21 \times 25 \text{ mm}^2$ . The effective width of the 21-mm dimension

expands to approximately 29 mm when wavelength dispersion of the full bandwidth is taken into account.

The spectral resolution of the system is achieved by using three  $110 \times 110\text{-mm}^2$ , 3600-line/mm holographic gratings. At a wavelength of 351 nm, the first-order diffraction efficiency is 38.8%. Based on a simulation of the spectrometer in OSLO,<sup>10</sup> a combination of the three gratings produces a total dispersion at the CCD detector in wavelength units per spatial distance of  $9.1 \times 10^{-2} \text{ pm}/\mu\text{m}$ .

The CCD detector is a scientific-grade,  $2048 \times 2048$  back-illuminated, thinned array.<sup>11</sup> The pixel pitch is  $13.5 \mu\text{m}$ .<sup>12</sup> To increase the sensitivity and eliminate any interference effects, the array has no protective window; therefore, the CCD is mounted in vacuum to protect the chip from degradation. Light enters the vacuum chamber through a window mounted at  $25^\circ$  to the optic axis so that any back-reflections from the CCD surface are removed from the FOV of the detector. The CCD is cooled to  $-30^\circ\text{C}$  to reduce dark noise. The smallest slit size should image to approximately  $8.7 \mu\text{m}$  at the detector plane,

Table 101.V: Specification of the optical system.

Optical Element	Position	Size (diameter for circular edge for square)	Specifications	Transmission
Slit	0.1 mm		10, 20, 40, 60 $\mu\text{m}$ Cr, AR	
Mirror	801.1 mm	150 mm on edge	HR 351 $23^\circ$ surface roughness 2.5 nm	0.995
Plano-concave collimation lens	1001.1 mm	192-mm diam $\times$ 30 mm thick	Radius 1 = $\infty$ Radius 2 = 368 mm	0.98
Convex-convex collimation lens	1105.2 mm	192-mm diam $\times$ 40 mm thick	Radius 1 = 524 mm Radius 2 = 473 mm	0.98
Mirror	1575.2 mm	150 mm on edge	HR 351 $27^\circ$ surface roughness 2.5 nm	0.995
Diffraction grating	2255.2 mm	110 mm	3600 gr/mm gold @ $45.5^\circ$	0.388
Diffraction grating	3015.2 mm	110 mm	3600 gr/mm gold @ $45.5^\circ$	0.388
Diffraction grating	3795.2 mm	110 mm	3600 gr/mm gold @ $45.5^\circ$	0.388
Mirror	4625.2 mm	150 mm on edge	HR 351 $37^\circ$ surface roughness 2.5 nm	0.995
Convex-convex focusing lens	4715.2 mm	192-mm diam $\times$ 40 mm thick	Radius 1 = 401 mm Radius 2 = 549 mm	0.98
Concave-plano focusing lens	4830.4 mm	192-mm diam $\times$ 30 mm thick	Radius 1 = 357 mm Radius 2 = $\infty$	0.98
Mirror	5050.4 mm	150 mm on edge	HR 351 $45^\circ$ surface roughness 2.5 nm	0.995
Vacuum window	5666.4 mm	50.8-mm diam $\times$ 5 mm thick	$25^\circ$ relative to normal incidence	0.992
CCD camera	5709.4 mm			0.17 (Q.E.)

which is less than the pixel pitch. Ideally, the image of a slit can illuminate just one pixel; however, the slit width must be convolved with the point-spread function listed above to determine the instrument resolution.

### Instrument Performance

The multichannel spectrometer is now operational on the OMEGA laser system, and the instrument performance can be compared with the design specifications. Figure 101.50 shows the image of an acquired laser shot. The first operational issue is calibrating the wavelength. The middle channel of the middle column can be illuminated with the light from a neon pencil lamp.<sup>13</sup> This channel is on the optical axis and has very small optical aberrations due to imperfections in the imaging system. In this configuration, four Ne I lines are visible.<sup>14</sup> A least-squares fit to those wavelengths yields an absolute wavelength calibration for the middle column and a relative calibration for the two outside columns.<sup>15</sup> The experimentally measured dispersion was  $8.6 \times 10^{-2}$  pm/ $\mu$ m, giving 1.16 pm/pixel. This is 6% lower than the modeled value listed above and indicates a slight offset in the position of lenses, which decreases the magnification. When the neon lamp illuminates the outside columns, not all of the lines are visible. To determine

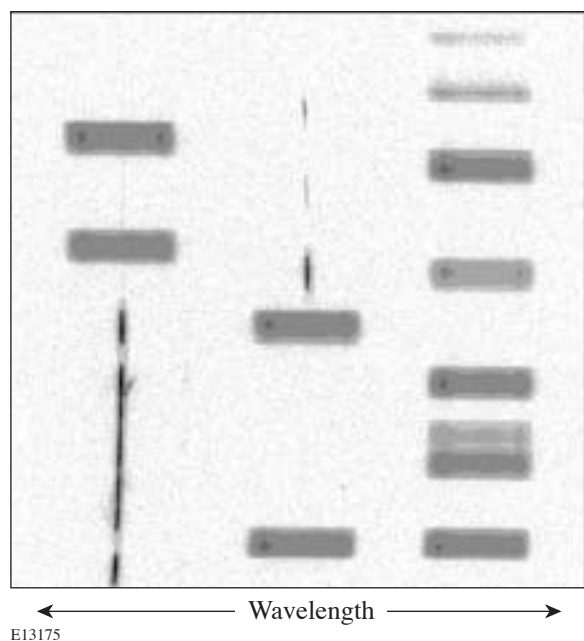


Figure 101.50

A UV-spectrometer CCD image from shot 37038 showing 23 of 60 beams with and without SSD. The density is logarithmic. The SSD beams, represented by large rectangular spectra, have approximately the same energy and 80 times the bandwidth of the narrow-linewidth beams.

the absolute calibration of the outside columns, the OMEGA laser is fired without the SSD bandwidth turned on. Under these conditions, all channels have the same narrow line spectrum. Adjusting the offset of the outside columns to match the center column gives an absolute wavelength calibration for all channels. The validity of the absolute wavelength calibration is tied to the precision to which the plate with the slit arrays can be reproducibly positioned. Since the illumination source is uniform, variations in the slit position translate to apparent shifts in the absolute wavelengths. The motorized, linear-translation stage can be reset to the same position to within 20  $\mu$ m, which implies that the wavelength calibration is accurate to approximately 2 pm after the slits are changed. To obtain the highest accuracy, the wavelength should be recalibrated every time the slit width is adjusted.

Aberrations within the imaging system of the spectrometer have been reduced to bring all channels within specifications. Channels near the optical axis exceed the performance requirements of the system. With SSD turned off, these channels will record a spectral full width at half maximum (FWHM) of 2.5 pm for laser energies that vary by a factor of 36 for 1-ns square pulses. The laser that seeds all sixty beams has a nearly transform-limited bandwidth, which has a measured UV-equivalent linewidth of less than 0.3 pm (the calculated linewidth of this laser is  $4 \times 10^{-4}$  pm). The independence of the spectral FWHM on laser energy implies that there is no *B*-integral broadening of the laser linewidth and the inputs to the spectrometer have the same spectral width as the seed laser; therefore, the measured linewidth is the intrinsic response of the instrument. For subnanosecond pulses, this is not the case. Figure 101.51 illustrates that the instrument performance is sufficient to observe *B*-integral broadening when it occurs. Two normalized spectra are shown: the wider spectrum is of a 100-ps pulse, the second spectrum is from a low-energy, 2-ns laser shot, which represents the instrument-limited response. As the position of the channels moves away from the optic axis, line-spread function increases. At the edges of the FOV of the CCD, the minimum FWHM is 6 pm. This resolution is sufficient for tuning the frequency-conversion crystals.

In addition to broadening, the optical system introduces curvature to the wavelength field. The straight slits in the object plane map to curves in the image plane, which deviate quadratically with distance from the center of the FOV. The maximum deviation at 14 mm from the optic axis is 300  $\mu$ m. With additional fine-tuning of the alignment, it might be possible to remove these aberrations. It was decided, however, that since the aberrations were sufficiently well characterized,

it was easier to remove them using image-processing algorithms than to realign the spectrometer.

The optical transmission through the spectrometer was measured by removing the fibers from the input to the spectrometer and recording the amount of light emerging from the fiber with a calibrated energy meter. The fiber was again connected to the spectrometer, and the total CCD analog-to-digital units (CCD\_ADU) were recorded. The CCD\_ADU total was converted to joules using the manufacturer's supplied quantum efficiency of the camera. A typical transmission value was  $1.6 \times 10^{-5} \pm 0.5 \times 10^{-5}$ , with most of the variation associated with the alignment of the fibers in the external fiber bundle with a similar internal fiber bundle that connects to the manifold. The transmission losses are dominated by the 10- $\mu\text{m}$  slit aperture on the 400- $\mu\text{m}$  source (transmission = 2.5%) and the mismatch between the  $f/2.5$  numerical aperture of the fibers coupling into the  $f/10$  of the collimating lens, which gives an effective transmission of 6%. The product of these transmissibilities is multiplied by the product of all the transmission factors listed in Table 101.V to estimate the transmission through the spectrometer as  $2.1 \times 10^{-5}$ . The light from a single channel that is transmitted to the CCD is very uniform in the spatial direction because of the homogenizer in the fiber manifold. There are 570 columns in each of the 63 spectra, and each of those 570 is the average of approximately 100 spatial pixels, all of which are nearly identical. The signal-to-noise

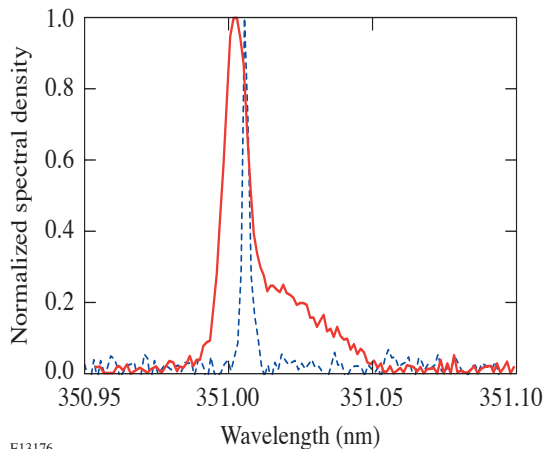


Figure 101.51  
The dashed curve represents a 9-J, 2-ns pulse on beam 61 (shot 35921). Under these conditions, the spectral width is expected to be transform limited. This curve represents the instrument response to a single frequency. The solid curve shows the broadening and spectral shift associated with a 50-J, 100-ps pulse (shot 36701).

ratio (SNR) at each point (the average over the column) is just the average divided by the standard deviation times the square root of the number of points averaged.<sup>16</sup> In a single image there are 35,910 individual measurements of the SNR. Figure 101.52 is a plot of the SNR as a function of the average signal in CCD\_ADU. This data was taken with SSD on and a 20- $\mu\text{m}$  slit. The peak SNR is 100 at an average signal of 300 ADU. Typical SSD spectra can be characterized as a flattop at 80% of the peak and a peak-to-valley modulation of 40% of the peak value. Over this range, most of the spectra have an SNR of 70 to 100. The SNR drops to 1 when the average pixel value is 1.4 ADU, so the dynamic range of this instrument is about 200. The solid line in Fig. 101.52 represents the SNR if the data followed Poisson statistics. At low signal counts, the SNR falls below this line due to the read noise of the CCD.

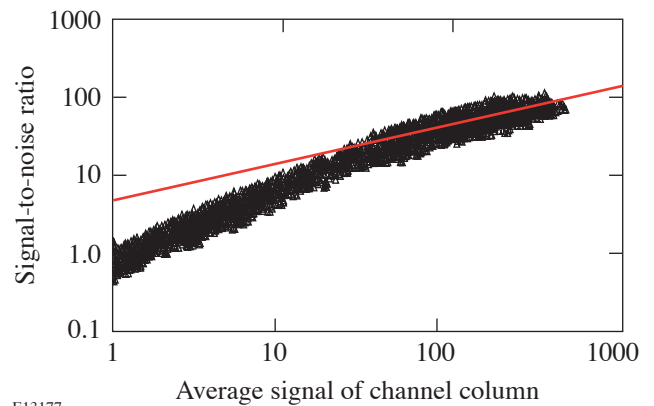


Figure 101.52  
The SNR ratio for each point in the image was calculated by dividing the average CCD\_ADU count in a 1-pixel-wide segment of a 100-pixel-high channel by the standard deviation of that same set of pixels times the square root of the number of pixels. These values are plotted as triangles. The solid line is the expected SNR of data following Poisson statistics.

A separate instrument records the energy of the UV light before it enters the fiber. The total CCD\_ADU for each channel has been correlated with this number, and the ratio is constant to within 8.5%. This is the precision to which the photometric calibration can be trusted. The precision is limited by crosstalk between the channels. Decreasing the channel width will decrease the crosstalk at the expense of the SNR.

Preliminary measurements with this instrument have verified that SSD spectra vary from beam to beam. A protocol is being developed to remove this variation by adjusting the angular tuning of the frequency-tripling KDP crystals. In

addition, the instrument is being used to study the spectral broadening that occurs in the OMEGA laser system when the pulse duration is less than 100 ps. The spectral shifts are closely tied to the rise and fall times of the pulse.

This spectrometer can prove to be a useful diagnostic instrument on large multibeam ICF laser systems such as LLE's OMEGA laser, the National Ignition Facility at Lawrence Livermore National Laboratory,<sup>17</sup> and the Le MegaJoule Laser in France,<sup>18</sup> where the bandwidth is deliberately added to the laser spectrum for spatial smoothing or for suppression of nonlinear processes such as stimulated Brillouin scattering. The spectrometer's unique design employing refractive optics makes it suitable for imaging spectroscopic applications that deal with relatively narrow spectroscopic ranges such as laser line broadening or for resolving a specific atomic transition.

#### ACKNOWLEDGMENT

This work was supported by the U.S. Department of Energy Office of Inertial Confinement Fusion under Cooperative Agreement No. DE-FC52-92SF19460, the University of Rochester, and the New York State Energy Research and Development Authority. The support of DOE does not constitute an endorsement by DOE of the views expressed in this article.

#### REFERENCES

1. T. R. Boehly, D. L. Brown, R. S. Craxton, R. L. Keck, J. P. Knauer, J. H. Kelly, T. J. Kessler, S. A. Kumpan, S. J. Loucks, S. A. Letzring, F. J. Marshall, R. L. McCrory, S. F. B. Morse, W. Seka, J. M. Soures, and C. P. Verdon, *Opt. Commun.* **133**, 495 (1997).
2. F. J. Marshall, J. A. Delettrez, R. Epstein, R. Forties, R. L. Keck, J. H. Kelly, P. W. McKenty, S. P. Regan, and L. J. Waxer, *Phys. Plasmas* **11**, 251 (2004).
3. M. D. Skeldon, *Rev. Sci. Instrum.* **71**, 3559 (2000).
4. S. Skupsky, R. W. Short, T. Kessler, R. S. Craxton, S. Letzring, and J. M. Soures, *J. Appl. Phys.* **66**, 3456 (1989).
5. R. S. Craxton, *Opt. Commun.* **34**, 474 (1980).
6. A. Babushkin, R. S. Craxton, S. Oskoui, M. J. Guardalben, R. L. Keck, and W. Seka, *Opt. Lett.* **23**, 927 (1998).
7. Y. R. Shen, *The Principles of Nonlinear Optics* (Wiley, New York, 1984), pp. 324–329.
8. Polymicro Technologies, Polymicro FVP 300 330 370, 2003, <http://www.polymicro.com> (4 August 2004).
9. J. P. Knauer, E. Pasch, G. Kühner, and the W7-AS Team, *Rev. Sci. Instrum.* **74**, 1679 (2003).
10. *OSLO User's Guide*, Version 5 (Sinclair Optics, Pittsford, NY 14534, 1996) (<http://www.sinopt.com>).
11. Spectral Instruments, Tucson, AZ 85745 (see <http://www.specinst.com/files/datasheets/4204-.pdf>).
12. e2v technologies, Elmsford, NY 10523-1482 (see <http://e2vtechnologies.com>).
13. T. Han *et al.*, *Rev. Sci. Instrum.* **74**, 2973 (2003).
14. NIST Atomic Spectra Database, NIST Standard Reference Database #78, 1999, [http://physics.nist.gov/cgi-bin/AtData/main\\_asd](http://physics.nist.gov/cgi-bin/AtData/main_asd) (4 August 2004).
15. M. Born and E. Wolf, *Principles of Optics: Electromagnetic Theory of Propagation, Interference and Diffraction of Light*, 6th ed. (Pergamon Press, Oxford, 1980), p. 436.
16. W. R. Donaldson, R. Boni, R. L. Keck, and P. A. Jaanimagi, *Rev. Sci. Instrum.* **73**, 2606 (2002).
17. E. I. Moses *et al.*, in *Optical Engineering at the Lawrence Livermore National Laboratory*, edited by T. T. Saito and M. A. Lane (SPIE, Bellingham, WA, 2003), Vol. 5001, pp. 1–15.
18. G. Thiell *et al.*, *Fusion Sci. Technol.* **43**, 478 (2003).